Three-Dimensional Correlation of Steric and Electronic Free Energy Relationships Guides Asymmetric Propargylation

Kaid C. Harper and Matthew S. Sigman

Science **333**, 1875 (2011);
DOI: 10.1126/science.1206997

Three-Dimensional Correlation of Steric and Electronic Free Energy Relationships Guides Asymmetric Propargylation

Kaid C. Harper and Matthew S. Sigman*

Chemical reaction outcomes are often rationalized on the basis of independent analyses of steric and electronic effects. We applied three-dimensional free energy relationships correlating steric and electronic effects to design and optimize a ligand class for the enantioselective Nozaki-Hiyama-Kishi propargylation of ketones. The resultant mathematical model describing the steric and electronic parameter relationship is highly reliant on the synergistic interactions of these two effects.

Complex chemical reactions can proceed through numerous pathways to many different products, although synthetic utility generally requires enrichment of a single product, presumably through a preferred low-energy pathway. This selectivity is commonly ascribed to two specific properties: electronic and steric effects. Electronic effects refer to variations in orbital electron density through bonding or spatial interactions (*1*). An electronic effect is a general term that can include inductive effects, conjugative (resonance) effects, or molecular orbital symmetry considerations. Steric effects arise from electrostatic repulsion as atoms or molecules approach each other, as commonly modeled by the Lennard-Jones potential (*1*–*4*).

Quantitative parameterization of electronic effects has been extensively used in physical organic chemistry as a means of probing reaction mechanisms, often by application of the Hammett σ-value framework (*5*, *6*). These parameters reflect the relative acidity of benzoic acid derivatives (Fig. 1) and are generally considered robust. In contrast, quantifying steric effects has been historically controversial, with several different sets of parameters developed over the years, each based on different measurable quantities or computations (*7*). Steric parameters introduced by Taft in the 1950s were derived from the relative rate of acid-catalyzed hydrolysis of methyl esters (Fig. 1), which were later correlated to the van der Waals radii of the substituent by Charton (*7*–*12*). The Taft-Charton steric parameters have seen the most extensive use, although debate on their validity continues (*7*).

The importance of both steric and electronic effects is magnified in asymmetric catalysis, where the diastereomeric transition states leading to enantiomerically enriched products can differ by as little as 1 to 3 kcal/mol. Of the two, steric effects, generally through the introduction of a large group to enhance repulsive interactions between a substituent(s) on the catalyst and the substrate, are most commonly implicated as an asymmetric catalyst design principle (*13*, *14*). However, electronic effects, both inductive and conjugative, can have an equally important impact on reaction enantioselectivity (*15*–*18*). Although computational techniques accounting for steric and electronic effects on asymmetric catalyst performance have made great strides over the past decade to aid catalyst design (*19*–*30*), it is difficult to implement these approaches for mechanistically and structurally ill-defined reactions (*31*, *32*). This is especially true for a priori understanding of catalyst electronic effects and their potential synergistic relationship to steric effects. Therefore, a practitioner of asymmetric catalyst development often relies on an independent qualitative evaluation of catalyst steric and electronic properties, although quantitative structure-selectivity relationships, analogous to the structure-activity approaches used in pharmaceutical optimization, have generally been used for ex post facto rationale of catalyst performance (*19*–*22*, *33*, *34*). Here, we describe a facile method to quantitatively and simultaneously probe steric and electronic effects, using basic principles of physical organic chemistry in the context of a chiral ligand class for enantioselective ketone propargylation.

Previous efforts in our group have focused on independently correlating electronic and steric effects as a function of catalyst substituent with the observed enantiomeric ratio (e.r.), which is directly proportional to the difference in transition state energies ($\Delta\Delta G^{\ddagger}$) (*18*, *35*–*38*). Although these efforts led to qualitative insight into important structural features responsible for asymmetric catalysis, extrapolation to (or identification of) new catalysts was challenging. Therefore, we developed a method to simultaneously examine and correlate the steric effects of two key ligand substituents through the use of mathematical surface models (*38*). This approach combines experimental design principles with the systematic synthesis of ligand libraries. Manipulation of the resultant surface models allowed for successful prediction of previously untested catalysts through extrapolation and conclusive identification of optimal catalysts for a given Nozaki-Hiyama-Kishi (NHK) carbonyl allylation, wherein a carbonyl-bearing substrate reacts with a Cr(III)-allyl species generated from the reaction of Cr(II) and an allyl halide (*39*). We were initially interested in expanding the use of this ligand-based design of experiments approach to other NHK-type reactions.

Of several possible reaction types, the NHK propargylation of ketones drew our interest because the homopropargylic tertiary alcohol products constitute a synthon for use in target-oriented synthesis (*40*). Shibasaki and colleagues (*41*) and Fandrick *et al*. (*42*) have recently and independently reported catalytic, enantioselective ketone propargylations via a Cu-catalyzed addition of boronic ester derivatives to ketones. Catalytic enantioselective propargylation of ketones using the commercially available and attractive propargyl halide reagents in the NHK protocol has not been reported. Therefore, we submitted the oxazoline-proline ligand library **3** to the enantioselective ketone propargylation using propargyl bromide (Fig. 2). A mathematical surface model (Eq. 1) was fit to the results:

$$\Delta\Delta G^{\ddagger} = -1.87 + 1.34X + 3.03Y - 0.99Y^2 - 1.19XY + 0.62XY^2 - 0.73YX^2 \quad (1)$$

Qualitative evaluation reveals a relatively shallow surface, with a predicted optimal catalyst

Fig. 1. Classic steric and electronic parameters in organic chemistry.

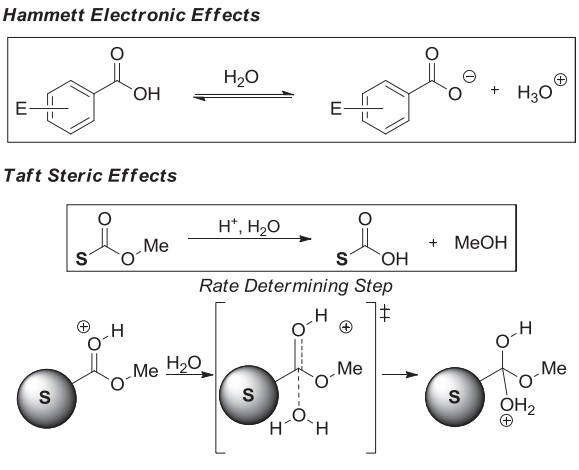

Department of Chemistry, University of Utah, Salt Lake City, UT 84112, USA.

*To whom correspondence should be addressed. E-mail: sigman@chem.utah.edu

performance of only 75:25 e.r. for this ligand scaffold. This modeling suggests that satisfactory enantioselectivity could not be achieved using this ligand class, and thus a different ligand scaffold was targeted.

To design a distinct ligand template, we opted to conserve the proline component of **3** because of its proven effectiveness in asymmetric catalysis and the relative ease with which its steric profile can be synthetically modulated (*43*, *44*). We replaced the oxazoline component to allow for the systematic evaluation of electronic parameters; we also incorporated a steric element into its substitute, motivated by the observed enhancement of enantioselectivity with larger oxazoline substituents, as seen for ligand **4** (Fig. 3A). Specifically, we selected aromatic heterocycles as a replacement allowing access to similar chelation environments about the Cr catalyst, while also allowing for systematic electronic perturbations. To test the viability of this ligand design, both the pyridine-proline and quinoline-proline ligands (**5** and **6a**, respectively) were synthesized and evaluated in the enantioselective NHK propargylation of acetophenone. Substituting pyridine for the oxazoline did not lead to improvement in enantioselectivity, but instead suggested that an aromatic heterocycle was a functional oxazoline analog of our previous catalyst system. Use of the larger heterocycle (**6a**), quinoline, yielded a higher e.r. for this difficult reaction class.

The quinoline-proline (QuinPro)–based ligand structure is perfectly suited to simultane-

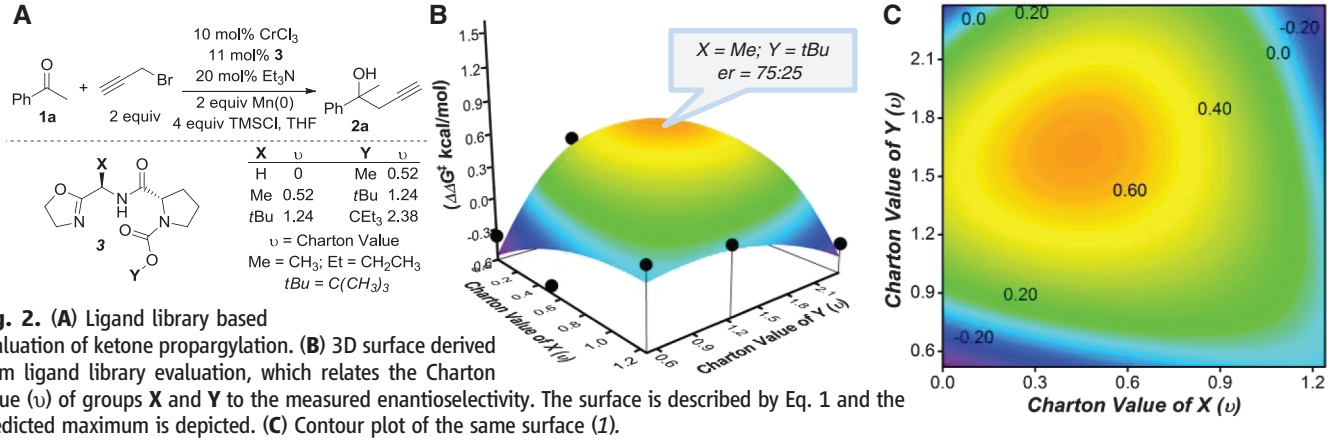

Fig. 2. (**A**) Ligand library based evaluation of ketone propargylation. (**B**) 3D surface derived from ligand library evaluation, which relates the Charton value (υ) of groups **X** and **Y** to the measured enantioselectivity. The surface is described by Eq. 1 and the predicted maximum is depicted. (**C**) Contour plot of the same surface (*1*).

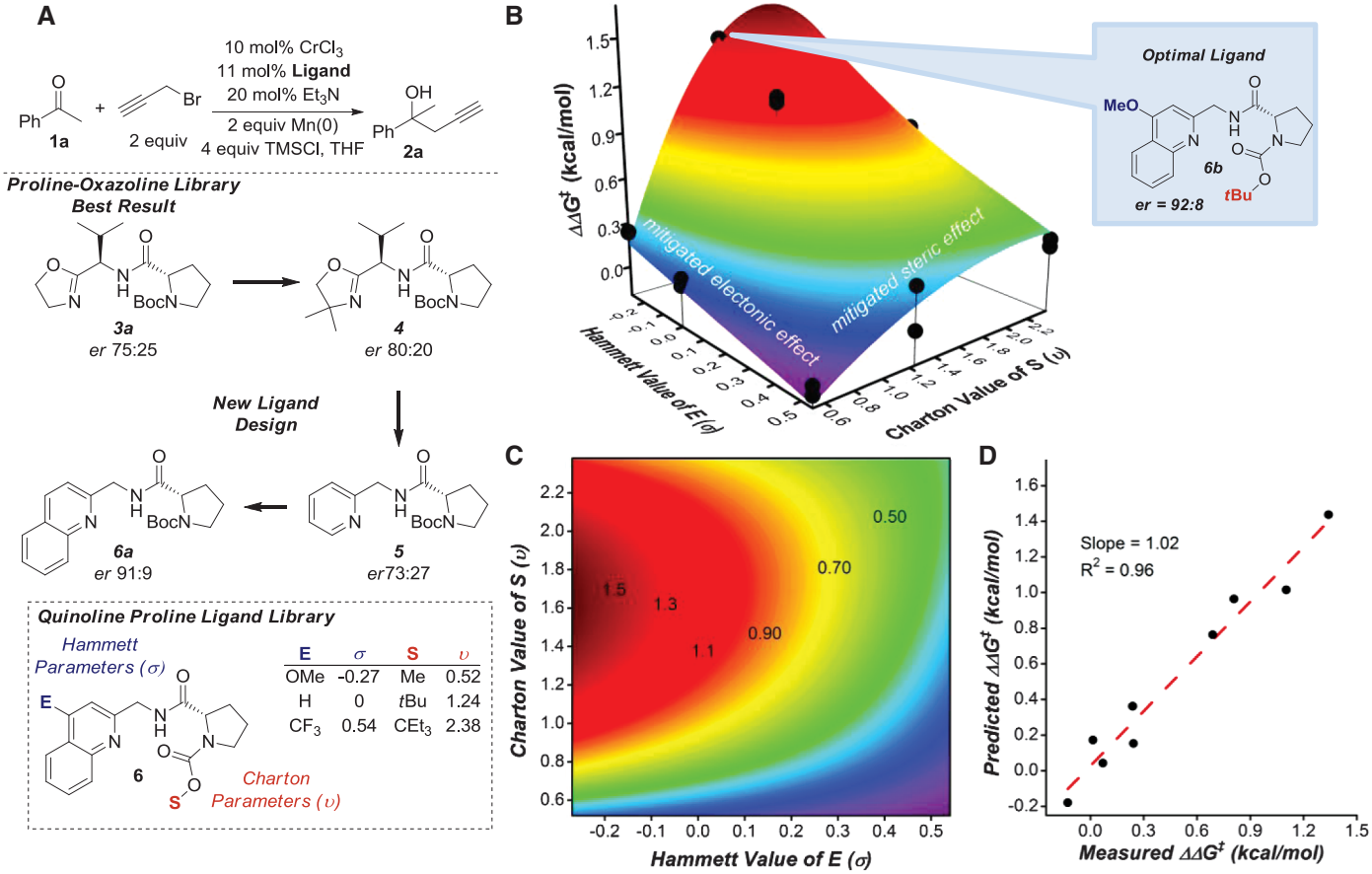

Fig. 3. (**A**) Ligand evolution for the Nozaki-Hiyama-Kishi propargylation of ketones, which led to the development of the QuinPro ligand scaffold. (**B**) Surface derived from the evaluation of the QuinPro library with replicate runs and modeled by Eq. 4 (raw data in table S2). (**C**) Contour plot of Eq. 4. (**D**) Comparison of the $\Delta\Delta G^{\ddagger}$ values predicted by Eq. 4 and the averaged measured value experimentally observed for each of the nine ligands in the QuinPro library.

ously optimize the effects of electronic and steric parameters. The ligand substituents that constitute the library were selected on the basis of experimental design principles, where the incorporation of substituents evenly spans a wide parameter range of both Hammett and Charton values (*5*, *6*, *9*–*12*). A nine-membered (3 × 3) ligand library was targeted to balance the synthetic effort with the statistical requirements for developing a three-dimensional (3D) model (*38*).

The desired ligands were synthesized and evaluated with replicates in the propargylation of acetophenone under the conditions specified in Fig. 3A (*45*). The data set required that a 3D surface function be developed to accurately model the data. From inspection of the raw data, we chose as the base function a full third-order polynomial (Eq. 2) that appeared to adequately describe the observed variation:

$$\Delta\Delta G^{\ddagger} = z0 + aE + bS + cE^2 + dS^2 + fES + gE^3 + hS^3 + iES^2 + jSE^2 \quad (2)$$

The data were arrayed into matrix format with the design matrix **X** (18 data points, nine individual ligands with their replicates, to allow for statistically meaningful modeling of the 10 parameters: 1, *E*, *S*, E^2, S^2, *ES*, E^3, S^3, ES^2, and SE^2) and the corresponding response matrix **Y** (18 × 1) of observed enantioselectivity. The polynomial base model was refined using backward elimination regression techniques, wherein terms were added to or omitted from the base polynomial function iteratively according to the magnitude of the covariance (error) associated with each term as verified by a *p* test. The design and response matrices were used to solve for the matrix of parameters (**C**) using the linear algebra definition of regression (Eq. 3) (*46*, *47*):

$$\mathbf{C} = (X^T X)^{-1}(X^T Y) \quad (3)$$

Equation 4 defines the model with the most statistical significance:

$$\Delta\Delta G^{\ddagger} = -1.20 + 1.22E + 2.84S - 0.85S^2 - 3.79ES + 1.25ES^2 \quad (4)$$

The surface in Fig. 3B describes this equation, and the resultant contour plot is depicted in Fig. 3C. Evaluation of the goodness of fit (Fig. 3D) shows good correlation of the original experimentally measured enantioselectivities with those output by the final model (predicted value). The optimal ligand as described by Eq. 4 lies nearest *E* = O-methyl (OMe), *S* = *tert*-butyl (*t*Bu). The relative ease of synthesis as well as the general availability of the ligand precursors makes this particular ligand desirable. Although this ligand is incorporated in the original data set, the combination of experimental design (evenly spreading the parameters over a large range) (*47*) and mathematical modeling of the data provides a high level of confidence that **6b** is the optimal ligand. If the optimal ligand were not incorporated into the original library, the modeling should allow for effective new catalyst selection, as previously reported (*38*). Finally, the QuinPro library was evaluated in the enantioselective propargylation of 2-hexanone, a model substrate for aliphatic ketones, where the same catalyst was found to be optimal.

The standard approach to asymmetric catalyst development is to evaluate catalyst properties independently and individually. Inspection of the data in Fig. 3B reveals that this approach would be unlikely to expose the synergy between the steric and electronic effects in this catalyst system. For example, steric effects are substantially mitigated for electron-poor ligands (*E* = CF_3), whereas a considerable enhancement of the steric effect is observed for electron-rich ligands (*E* = OMe). Furthermore, the electronic effect for smaller substituents (*S* = Me) is diminished as compared to the effect observed for the series containing *S* = *t*Bu. Simply put, a poor choice of one variable could not be superseded by an ideal choice in the other.

This empirical inspection is strongly reinforced by the derived mathematical model described in Eq. 4. Inclusion of crossterms between the putatively independent variables not only considerably improves the model, but also mathematically defines a significant synergistic relationship between the electronic and steric interactions in the catalyst. Specifically, the terms *ES* and ES^2 suggest that the electronic nature of the catalyst and the steric environment in the transition state are closely correlated. Because the electronic variable itself contains no chiral information, the electronic effect on enantioselectivity presumably is through mitigation of the Lewis acidity of the Cr center.

Noting that both aromatic and aliphatic ketones remain difficult substrate classes for these carbonyl addition reactions, we first explored the substrate scope by evaluating various aryl ketone substrates using ligand **6b** (Fig. 4). Generally,

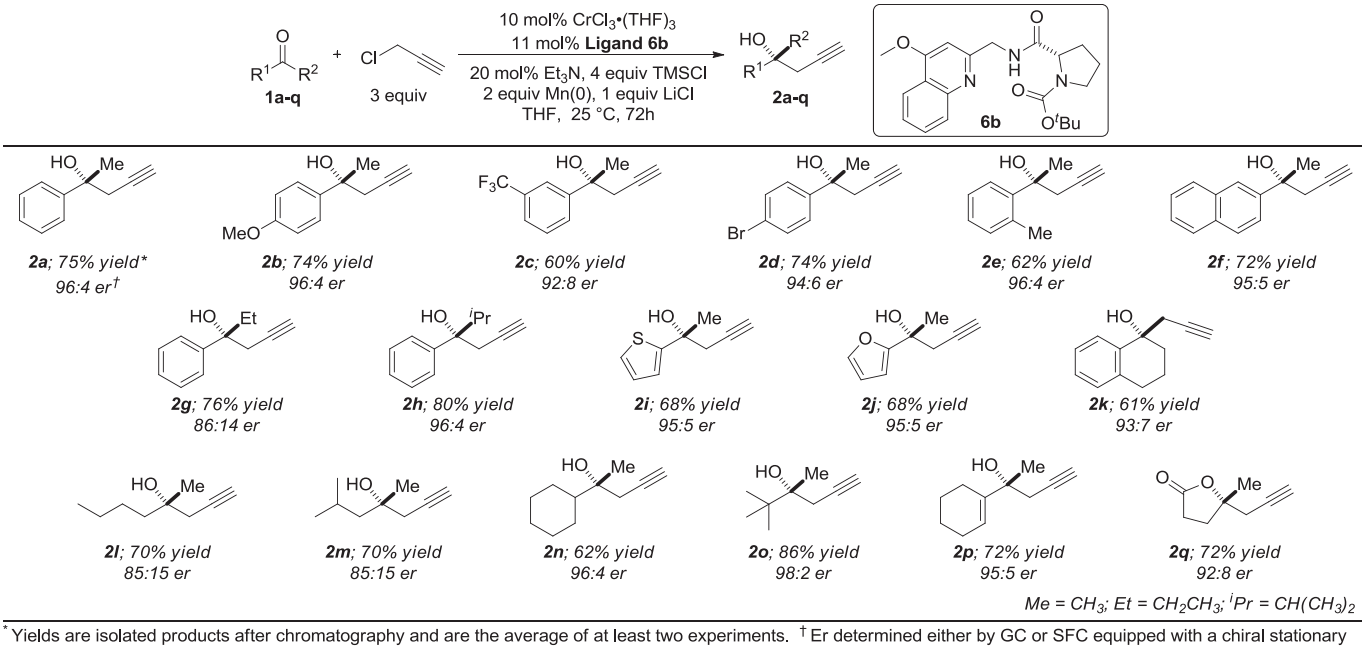

*Yields are isolated products after chromatography and are the average of at least two experiments. †Er determined either by GC or SFC equipped with a chiral stationary phase. Absolute configuration of **2f** and **2p** was determined by comparison to known compounds and all others through analogy (see supporting online material).

Fig. 4. Substrate scope of the enantioselective ketone propargylation reaction.

high enantioselectivity and good yield were observed for aryl methyl ketones, with a modest drop in enantioselectivity for electron-poor substrates. Other aryl ketones gave rise to good to excellent e.r.'s, as highlighted by substrate **2h**. Heteroaromatics were also well tolerated under the reaction conditions, with thiophene- and furan-derived ketones undergoing highly enantioselective propargylation reactions (**2i** and **2j**). Additionally, an α,β-unsaturated ketone was an excellent substrate for enantioselective propargylation, leading to a 95:5 e.r. (**2p**).

In the case of aliphatic ketones, the catalyst selected on the basis of steric differentiation, giving higher e.r.'s with increased steric bulk on a single side of the ketone (**2l** to **2o**). An e.r. of 85:15 observed for 2-hexanone (**2l**) is relatively impressive, considering that the catalyst is differentiating a methyl from an *n*-butyl group. Groups with substitution at the α-position of the ketone substantially enhanced the e.r.'s, as highlighted by ketones with a cyclohexyl (96:4 e.r., **2n**) and a *t*-butyl group (98:2 e.r., **2o**). Furthermore, a γ-butyrolactone (**2q**) could be synthesized with a good e.r. from propargylation of an aliphatic ketone with a pendant ester.

Our data suggest that steric-electronic correlations provide a means for efficient optimization of a catalytic system and are evidence for a synergistic relationship between these two classically independent variables in reactions. This is especially attractive for optimizing reactions with limited detailed mechanistic and structural understanding and, considering that the modeling is tied to basic physical organic precepts, a greater understanding of the underlying features of asymmetric catalysis should result. The application of this method is not limited to asymmetric catalysis but can potentially be applied to broad areas of chemistry dependent on evaluating the interplay of two (or more) effects on a reaction outcome.

References and Notes

1. E. V. Anslyn, D. A. Dougherty, in *Modern Physical Organic Chemistry*, J. Murdzek, Ed. (University Science, Sausalito, CA, 2006), pp. 441–482.
2. M. S. Newman, Ed., *Steric Effects in Organic Chemistry* (Wiley, New York, 1956).
3. J. E. Jones, *Proc. R. Soc. London Ser. A* **106**, 441 (1924).
4. J. E. Jones, *Proc. R. Soc. London Ser. A* **106**, 463 (1924).
5. L. P. Hammett, *J. Am. Chem. Soc.* **59**, 96 (1937).
6. C. Hansch, A. Leo, R. W. Taft, *Chem. Rev.* **91**, 165 (1991).
7. C. Hansch, A. Leo, in *Exploring QSAR: Fundamentals and Applications in Chemistry and Biology*, S. R. Heller, Ed. (American Chemical Society, Washington, DC, 1995), pp. 69–96.
8. R. W. Taft Jr., *J. Am. Chem. Soc.* **74**, 3120 (1952).
9. M. Charton, *J. Am. Chem. Soc.* **97**, 1552 (1975).
10. M. Charton, *J. Am. Chem. Soc.* **97**, 3691 (1975).
11. M. Charton, *J. Am. Chem. Soc.* **97**, 3694 (1975).
12. M. Charton, *J. Org. Chem.* **41**, 2217 (1976).
13. E. N. Jacobsen, A. Pfaltz, H. Yamamoto, Eds., *Comprehensive Asymmetric Catalysis I-III* (Springer, New York, 1999).
14. P. J. Walsh, M. C. Kozlowski, in *Fundamentals of Asymmetric Catalysis*, J. Murdzek, Ed. (University Science, Sausalito, CA, 2009), pp. 1–240.
15. A. L. Casalnuovo, T. V. RajanBabu, T. A. Ayers, T. H. Warren, *J. Am. Chem. Soc.* **116**, 9869 (1994).
16. D. W. Nelson *et al*., *J. Am. Chem. Soc.* **119**, 1840 (1997).
17. M. Palucki *et al*., *J. Am. Chem. Soc.* **120**, 948 (1998).
18. K. H. Jensen, M. S. Sigman, *J. Org. Chem.* **75**, 7194 (2010).
19. M. C. Kozlowski, S. L. Dixon, M. Panda, G. Lauri, *J. Am. Chem. Soc.* **125**, 6614 (2003).
20. M. C. Kozlowski, M. Panda, *J. Org. Chem.* **68**, 2061 (2003).
21. J. C. Ianni, V. Annamalai, P.-W. Phuan, M. Panda, M. C. Kozlowski, *Angew. Chem.* **118**, 5628 (2006).
22. K. B. Lipkowitz, C. A. D'Hue, T. Sakamoto, J. N. Stack, *J. Am. Chem. Soc.* **124**, 14255 (2002).
23. S. J. Zuend, E. N. Jacobsen, *J. Am. Chem. Soc.* **131**, 15358 (2009).
24. C. Uyeda, E. N. Jacobsen, *J. Am. Chem. Soc.* **133**, 5062 (2011).
25. S. J. Zuend, E. N. Jacobsen, *J. Am. Chem. Soc.* **129**, 15872 (2007).
26. P.-O. Norrby, T. Rasmussen, J. Haller, T. Strassner, K. N. Houk, *J. Am. Chem. Soc.* **121**, 10186 (1999).
27. P. H.-Y. Cheong, C. Y. Legault, J. M. Um, N. Çelebi-Ölçüm, K. N. Houk, *Chem. Rev.* **111**, 5042 (2011).
28. K. B. Lipkowitz, M. Pradhan, *J. Org. Chem.* **68**, 4648 (2003).
29. P. J. Donoghue, P. Helquist, P.-O. Norrby, O. Wiest, *J. Chem. Theory Comput.* **4**, 1313 (2008).
30. P. J. Donoghue, P. Helquist, P.-O. Norrby, O. Wiest, *J. Am. Chem. Soc.* **131**, 410 (2009).
31. C. Allemann, R. Gordillo, F. R. Clemente, P. H.-Y. Cheong, K. N. Houk, *Acc. Chem. Res.* **37**, 558 (2004).
32. T. Dudding, K. N. Houk, *Proc. Natl. Acad. Sci. U.S.A.* **101**, 5770 (2004).
33. S. E. Denmark, N. D. Gould, L. M. Wolf, *J. Org. Chem.* **76**, 4337 (2011).
34. J. D. Oslob, B. Åkermark, P. Helquist, P.-O. Norrby, *Organometallics* **16**, 3015 (1997).
35. M. S. Sigman, J. J. Miller, *J. Org. Chem.* **74**, 7633 (2009).
36. J. L. Gustafson, M. S. Sigman, S. J. Miller, *Org. Lett.* **12**, 2794 (2010).
37. J. J. Miller, M. S. Sigman, *Angew. Chem. Int. Ed.* **47**, 771 (2008).
38. K. C. Harper, M. S. Sigman, *Proc. Natl. Acad. Sci. U.S.A.* **108**, 2179 (2011).
39. The resultant Cr(III)-alkoxide releases product through reaction with TMSCl and Mn subsequently reduces the catalyst to Cr(II).
40. C.-H. Ding, X.-L. Hou, *Chem. Rev.* **111**, 1914 (2011).
41. S.-L. Shi, L.-W. Xu, K. Oisaki, M. Kanai, M. Shibasaki, *J. Am. Chem. Soc.* **132**, 6638 (2010).
42. K. R. Fandrick *et al*., *J. Am. Chem. Soc.* **133**, 10332 (2011).
43. B. List, *Tetrahedron* **58**, 5573 (2002).
44. J. J. Miller, M. S. Sigman, *J. Am. Chem. Soc.* **129**, 2752 (2007).
45. Table S2 contains the raw data used to initiate the modeling process.
46. See supporting material on *Science* Online.
47. S. N. Deming, S. L. Morgan, *Experimental Design: A Chemometric Approach* (Elsevier, New York, ed. 2, 1993).

Acknowledgments: Supported by NSF grant CHE-0749506.

Supporting Online Material

www.sciencemag.org/cgi/content/full/333/6051/1875/DC1
Materials and Methods
Tables S1 to S26
References (*48*, *49*)

14 April 2011; accepted 13 July 2011
10.1126/science.1206997

Diurnal and Seasonal Mood Vary with Work, Sleep, and Daylength Across Diverse Cultures

Scott A. Golder* and Michael W. Macy

We identified individual-level diurnal and seasonal mood rhythms in cultures across the globe, using data from millions of public Twitter messages. We found that individuals awaken in a good mood that deteriorates as the day progresses—which is consistent with the effects of sleep and circadian rhythm—and that seasonal change in baseline positive affect varies with change in daylength. People are happier on weekends, but the morning peak in positive affect is delayed by 2 hours, which suggests that people awaken later on weekends.

Individual mood is an affective state that is important for physical and emotional well-being, working memory, creativity, decision-making (*1*), and immune response (*2*). Mood is influenced by levels of dopamine, serotonin, and other neurochemicals (*1*), as well as by levels of hormones (e.g., cortisol) (*3*). Mood is also externally modified by social activity, such as daily routines of work, commuting, and eating (*4*, *5*). Because of this complexity, accurate measurement of affective rhythms at the individual level has proven elusive.

Experimental psychologists have repeatedly demonstrated that positive and negative affect are independent dimensions. Positive affect (PA) includes enthusiasm, delight, activeness, and alertness, whereas negative affect (NA) includes distress, fear, anger, guilt, and disgust (*6*). Thus, low PA indicates the absence of positive feelings, not the presence of negative feelings.

Laboratory studies have shown that diurnal mood swings reflect endogenous circadian rhythms interacting with the duration of prior wakefulness or sleep. The circadian component corresponds to change in core body temperature, which is lowest at the end of the night and peaks during late afternoon. The sleep-dependent component is elevated at waking and declines throughout the day (*7*). Other studies have variously observed a single PA peak 8 to 10 hours after waking (*8*), a

Department of Sociology, Cornell University, Ithaca, NY 14853, USA.

*To whom correspondence should be addressed. E-mail: sag262@cornell.edu